

The origin of extensional flow in a channel with sudden contraction and expansion

I V Kravchenko¹, S A Patlazhan², R Muller³ and V G Sultanov¹

¹ Institute of Problems of Chemical Physics of the Russian Academy of Sciences, Academician Semenov Avenue 1, Chernogolovka, Moscow Region 142432, Russia

² Semenov Institute of Chemical Physics of the Russian Academy of Sciences, Kosygina 4, Moscow 119991, Russia

³ Charles Sadron Institute UPR 22 CNRS, 23 rue du Loess, Strasbourg 67034, France

E-mail: sapat@yandex.ru

Abstract. The pressure driven flow of a viscous incompressible fluid in a 2D channel with sudden contraction and expansion is investigated numerically. The attention is concentrated on studying conditions of occurrence of the elongational flow in a narrow section of the channel. To this end, interconnection between flow patterns and axial velocities is analyzed at different Reynolds numbers.

1. Introduction

The viscous fluid flow in a channel with variable contraction and expansion areas is accompanied by a number of hydrodynamic effects: multiple bifurcation transitions from axially symmetric to steady-state asymmetric flow patterns and then to turbulent flow, can be observed under moderate increase in the Reynolds number [1–3]. The ability to control flow regimes by varying the geometrical and hydrodynamic parameters of the channel is exploited in intensification of the heat exchange [4, 5] and efficiency of chemical reactors [6, 7]. In recent years, convergent-divergent channels were used to produce a fine structure of micro- and nanocomposites based on immiscible polymer blends or filled polymers [8–11]. The latter is associated with the possibility of occurrence of elongation flow in the narrow part of the channel. In this case the velocity gradient is directed along the channel axis, causing breaking of the dispersed phase of a multiphase fluid at much lower Reynolds numbers as compared with the Poiseuille flow [12–14]. Furthermore, in contrast to shearing, elongational flow enables to split a dispersed phase of much higher relative viscosity. Nevertheless, the origin of formation of this type of flow in a channel with sudden contraction and expansion is still poorly understood.

Hitherto, attention was mainly focused on studying the flow behavior in large section chambers of the channel. Particularly, it was found that the vortex-free flow arises at very low fluid velocity, whereas increasing of the Reynolds number leads to formation of symmetrical vortices in the downstream chamber. Above a certain critical Reynolds number the dimensions of the corner vortices begin to differ. The reason for this effect is the flow instability with regards to fluctuations of the velocity field. As a result, under- and overpressure zones are formed near the opposing walls of the channel giving rise to a secondary cross current and, consequently, to violation of flow symmetry. A further increase in the Reynolds number stimulates the appearance



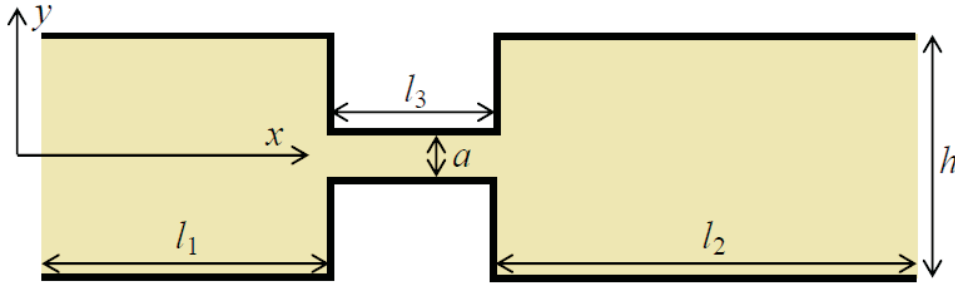


Figure 1. Channel with the sudden contraction expansion.

of new vortices and then the failure of a steady-state asymmetrical flow followed by transition to the unsteady vortex flow. These phenomena are characteristic of both pressure- and piston-driven flow [1, 2, 15].

Mathematical modeling has shown that flow patterns in the central longitudinal section of a sufficiently thick 3D rectangular channel coincide with predictions of a 2D model of a channel with the same contraction ratio of the transversal dimensions of the broad and narrow portions of the channel [2, 3]. Therefore, to describe flow peculiarities in the narrow zone of the channel it is sufficient to consider a simple 2D model. This approach is also useful to shorten numerical calculation time and to facilitate analysis of the obtained data.

In this communication we present results of numerical modeling of the pressure driven viscous flow through a 2D channel containing a narrow part between two broad chambers. The flow peculiarities at different Reynolds numbers are studied with the aim of understanding conditions of occurrence of the elongational flow.

2. Theoretical background

The geometry of the considered computational domain of the channel is shown in figure 1. Its contraction ratio is taken as $CR = h/a = 15$ which corresponds to a laboratory mixer RMX[®], used for processing of immiscible polymer blends and emulsions [11]. Considering the width of the narrow part of the channel $a = 0.002$ m as a unit length, the other dimensionless characteristics presented in figure 1 are equal to $l_1 = 75$, $l_2 = 225$ and $l_3 = 5$. We study the flow of an incompressible Newtonian fluid with kinematic viscosity $\nu = 10^{-5}$ m²/s (the dynamic viscosity and density are respectively taken as $\eta = 10^{-2}$ Pa·s and $\rho = 10^3$ kg/m³).

The velocity field $\mathbf{u} = (u, v)$ of the incompressible fluid is governed by the Navier–Stokes equation

$$\rho \left(\frac{\partial \mathbf{u}}{\partial t} + (\mathbf{u} \cdot \nabla) \mathbf{u} \right) = -\nabla p + \eta \Delta \mathbf{u}. \quad (1)$$

The fluid velocity on the channel walls is zero (no-slip boundary condition). Equation (1) was solved numerically by means of separation of velocity and pressure using the PISO algorithm of the computing platform OpenFOAM [16]. The finite volume method was used. Its essence is to divide the original area to a set of control volumes (mesh cells), in the centers of which stood the unknown variables. To this end, the computational domain was divided into three parts corresponding to the broad and narrow channel regions, on which were superimposed square grids with respective number of cells: 256×64 , 64×64 , and 1024×64 . The analysis showed that increasing the mesh density does not lead to a noticeable change in the solutions obtained and therefore this level of discretization seems to be optimal from the point of view of use of computational resources and calculation time. Integration of equation (1) was carried out on each finite volume. Then using the Gauss theorem, the volume integrals from the convective

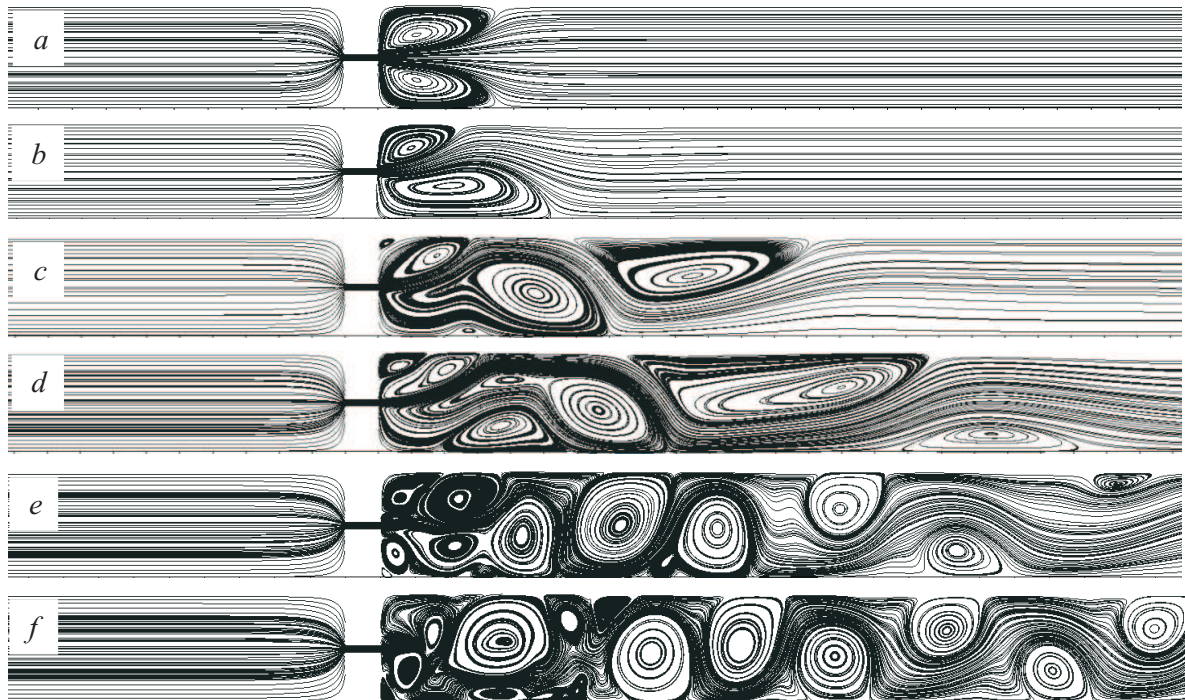


Figure 2. Pressure-driven streamlines in the channel with contraction ratio $CR = 15$ at different Reynolds numbers: $Re = 20.0$ (a), 23.6 (b), 62.0 (c), 101.8 (d), 180.6 (e), 268.0 (f).

and diffusive terms were replaced by surface integrals. The linear equations obtained while their sampling were solved by means of iteration procedure.

3. Results and discussion

Flow regimes in the channel with the given aspect ratio $CR = 15$ are determined by the value of the Reynolds number. It was determined as $Re = \rho u_{\max} a \eta^{-1}$ with u_{\max} corresponding to the maximum velocity in the contracted section. Figure 2 shows the streamlines for Re values between 20 and 268. This range of Reynolds numbers is obtained for the pressure drop in the range from 0.025 to 1 Pa.

The flow patterns indicate several bifurcation transitions occurring with the increase of the Reynolds number. They start from the symmetric flow pattern with two identical angular vortices at $Re = 20.0$ (figure 2a) which transforms to asymmetric flows with two ($Re = 23.6$, figure 2b) and three ($Re = 62.0$, figure 2c) unequal vortices respectively, and then to the multiple vortex flow ($Re = 101.6$, figure 2d; $Re = 180.8$, figure 2e and $Re = 268.0$, figure 2f). These transitions were found to be reached after certain lag times [17]. The transient flow preceding the steady-state flow regime is of fundamental interest in terms of understanding the conditions of stability of a liquid jet leaving the narrow channel section into the downstream chamber. The first three flow regimes characterized by the existence of two and three vortices were found to eventually reach a steady state, while further increase in vortex number at larger values of Re results in unsteady or chaotic flow in the downstream chamber. So, the symmetric and asymmetric steady state flows are inherent to low and moderate Reynolds numbers while the unsteady vortex flow requires higher Re values. It should be mentioned that the pressure field is homogeneous at low Reynolds numbers both in the upstream and downstream chambers, while

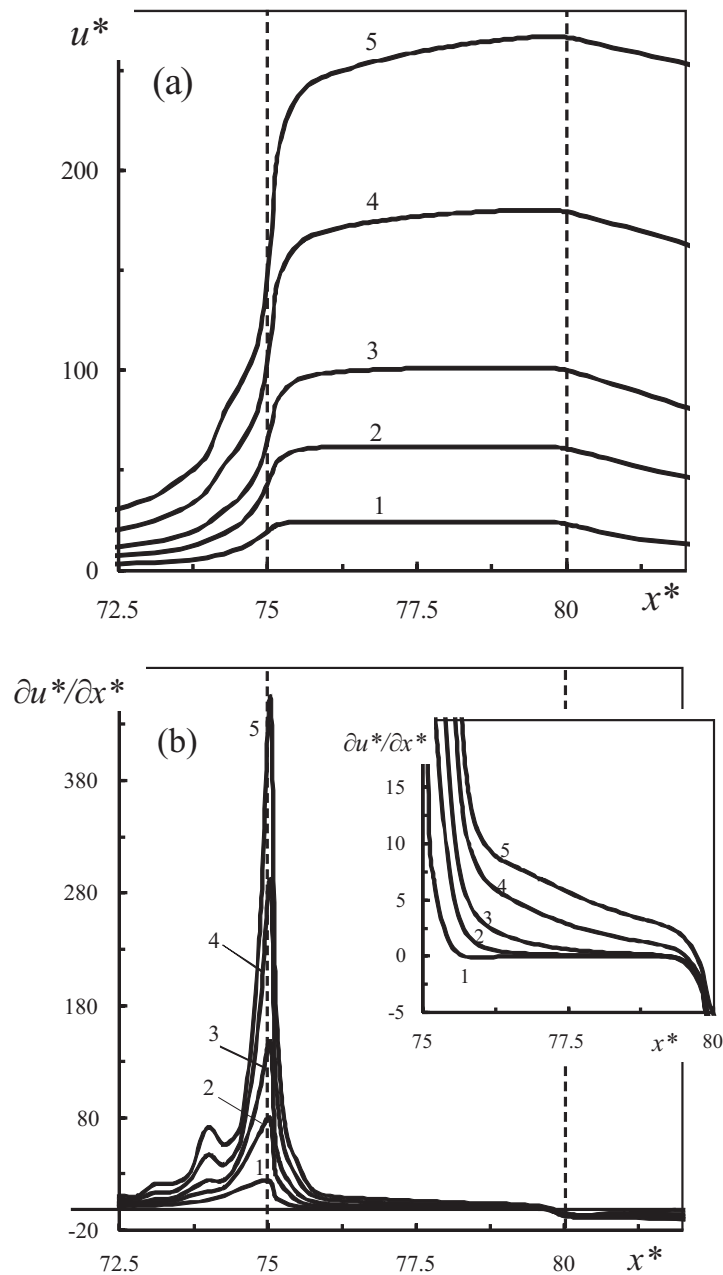


Figure 3. Variations of the dimensionless axial velocity u^* (a) and its gradient $\partial u^* / \partial x^*$ (b) at different Reynolds numbers: $Re = 23.6$ (1), 62.0 (2), 101.8 (3), 180.6 (4), 268.0 (5). The dashed lines indicate limits of the narrow part of the channel. The inset shows magnification of the velocity gradient within the confined area.

it becomes inhomogeneous and even unstable in the case of the asymmetric and chaotic vortex flows, respectively. Alternation of large and low pressure domains may play an important role in dispersion processes of multiphase fluids.

It is instructive to compare the calculated flow patterns with the behavior of velocity and pressure in the narrow part of the channel. Figure 3 shows changes of the horizontal component of the axial velocity and its longitudinal gradient for different Reynolds numbers. The results

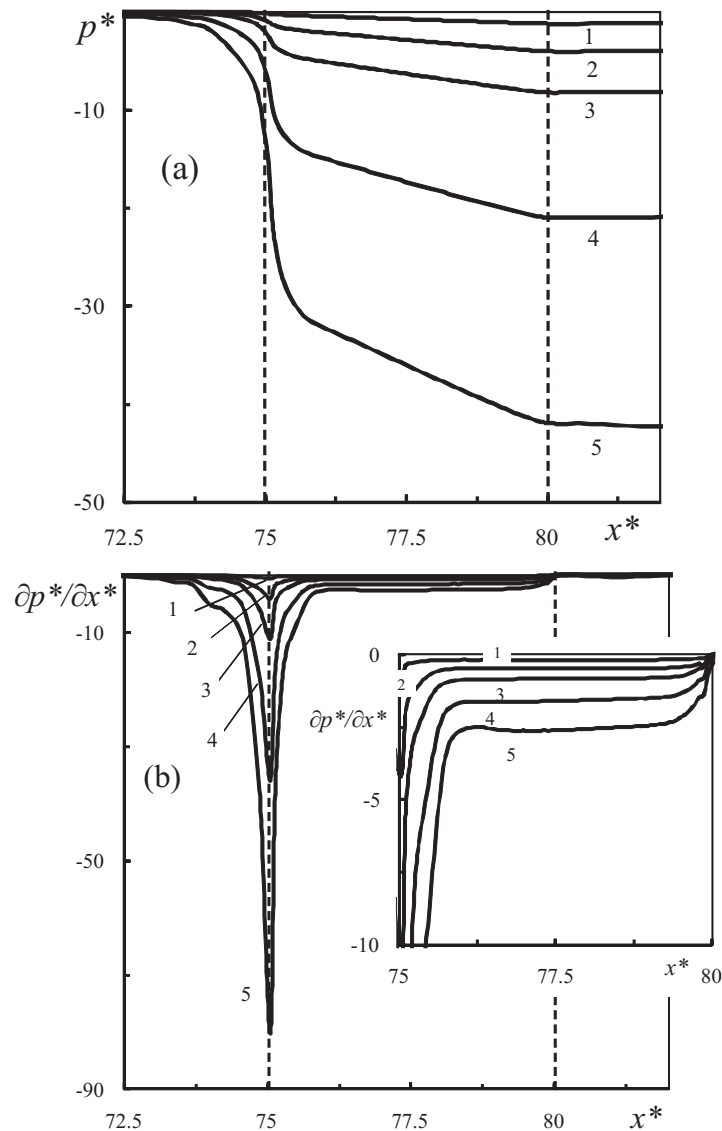


Figure 4. Variations of the dimensionless pressure p^* (a) and its longitudinal gradient $\partial p^*/\partial x^*$ (b) at different Reynolds numbers: $Re = 23.6$ (1), 62.0 (2), 101.8 (3), 180.6 (4), 268.0 (5). The dashed lines indicate limits of the narrow part of the channel. The inset shows magnification of the pressure gradient within the confined area.

are presented in the dimensionless form, where $u^* = ua/\nu$ and $x^* = x/a$. The narrow section of the channel is bounded by the dashed lines. It can be seen that the largest variations of velocity occur in the vicinity of the entrance of the narrow section, while near its exit the changes are insignificant. At low Reynolds numbers corresponding to the symmetric and double-vortex flows (figures 2a and 2b), the axial velocity increases slightly, and then quickly goes to its steady value. A different behavior shows up with further increase of the Reynolds number: the zone of constant axial velocity along the narrow section of the channel begins shrinking. This is illustrated in the inset to figure 3b showing a reduction of the length corresponding to the zero value velocity gradient. In the case of the unsteady vortex flow this zone disappears completely thus leading to the elongational flow through the entire length of the channel narrow section (see figures 2e

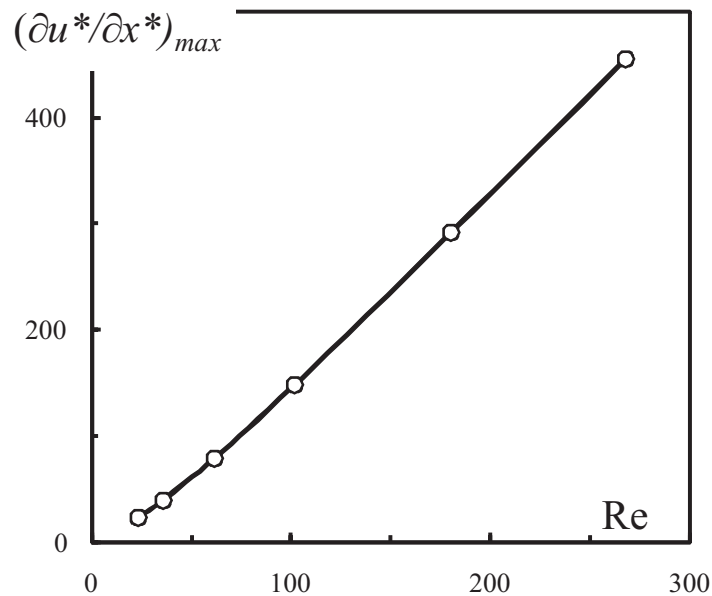


Figure 5. Dependence of maximum of the longitudinal velocity gradient $(\partial u^*/\partial x^*)_{\max}$ on Reynolds number.

and 2f). Being applied to processing of immiscible polymer blends or emulsions, the latter flow regimes are more suitable because the residence time in the elongational stream is increased appreciably.

The jump of longitudinal velocity gradient at the entrance of the narrow channel is caused by the sharp pressure drop in this zone. After that, the pressure gradient flattens out. These effects are demonstrated in figure 4 in terms of the dimensionless pressure $p^* = p\rho a^2/\eta^2$. However, at $Re = 180.6$ and 268.0 , corresponding to figures 2e and 2f, a weak growth of $\partial p^*/\partial x^*$ can be observed along the channel axis (see inset in figure 4b). This is quite sufficient to induce a longitudinal velocity gradient along the channel axis (curves 4 and 5 in figure 3b).

Considering the dependence of $(\partial u^*/\partial x^*)_{\max}$ on the Reynolds number at the entrance of the narrow section, it can be concluded that it is nearly linear function (see figure 5). This result can greatly simplify the choice of general flow conditions for obtaining the required properties of the elongational flow. Note that the presence of the longitudinal velocity gradient in the narrow part of the channel indicates deviation of the velocity profile from the parabolic shape typical for the Poiseuille flow. Calculations have shown that a plug flow takes place near the entrance to the narrow section. Then, closer to the exit, the plug flow is transformed to the Poiseuille flow at $Re < 100$, while at higher Reynolds numbers the parabolic velocity profile could never be reached (cf. inset to figure 3b).

It should be noted that present numerical modeling was performed as applied to 2D model of RMX[®] mixer with the given contraction ratio $CR = 15$ [11] (figure 1). The obtained results were found should correspond to a sufficiently thick 3D channel with the same contraction ratio [2, 3]. The symmetric vortex flow shown in figure 2a is similar to the flow pattern observed in RMX[®] at low Reynolds number [18]. The published experimental and numerical studies correspond to channels with different contraction ratios [1–3]. For this reason, comparison of our calculations with currently available experimental data may be done just qualitatively. These data indicate certain general regularities in formation of a flow structure. Particularly, the bifurcational transitions from the symmetric to asymmetric flow patterns were observed at

different CR values. Our findings are in line with these observations. Specifically, figures 2a and 2b show transition from the axially symmetric to the asymmetric vortex flow. Moreover, the critical Reynolds number of this transition at $CR = 15$ [17] corresponds to the predicted for the close contraction ratio [2].

4. Conclusions

The pressure driven flow of a viscous incompressible fluid in a 2D channel with sudden contraction and expansion were studied numerically. The flow patterns were found to vary from the steady symmetric and asymmetric patterns to the unsteady chaotic vortex flow with increase in the Reynolds number. The transitions result in the formation of the elongation flow in a narrow section of the channel. The sharp increase in the longitudinal velocity gradient at the entrance of the contraction zone is followed by its constant value increasing with the Reynolds number. This may play a crucial role in dispersion of multiphase fluids.

Acknowledgments

The work has been supported by the Russian Foundation for Basic Research (grant No.13-03-00725). Numerical calculations were carried out on the computing resources of the Joint Supercomputer Center of the Russian Academy of Sciences.

References

- [1] Durst F, Melling A and Whitelaw J H 1974 *J. Fluid Mech.* **64** 111–128
- [2] Oliveira M S N, Rodd L E, McKinley G H and Alves M A 2008 *Microfluid. Nanofluid.* **5** 809–826
- [3] Tsai C H, Chen H T, Wang Y N, Lin C H and Fu L M 2007 *Microfluid Nanofluid* **3** 13–18
- [4] Konoplev A A, Aleksanyan G G, Rytov B L and Berlin A A 2015 *Theor. Found. Chem. Eng.* **49** 61–69
- [5] Motaharinezahad M, Shahraki S, Tirgar R and Bisadi H 2014 *Indian J. Sci. Res.* **1** 47–53
- [6] Minsker K S, Berlin A A, Zakharov V P and Zaikov G E 2004 *Fast Liquid-Phase Processes in Turbulent Flows, Hoboken* (Boston: Taylor & Francis)
- [7] Dong L and Shufen Z 2014 *Int. J. Chem. React. Eng.* **12** 465–475
- [8] Luciani A and Utracki L A 1996 *Int. Polym. Proc.* **11** 299–309
- [9] Meller M, Luciani A and Manson J A E 2002 *Polym. Eng. Sci.* **42** 634–653
- [10] Tokihisa M, Yakemoto K, Sakai T A, Utracki L, Sepehr M, Li J and Simard Y 2006 *Polym. Eng. Sci.* **46** 1040–1050
- [11] Rondin J, Bouquey M, Muller R, Serra C A, Martin G and Sonntag P 2014 *Polym. Eng. Sci.* **54** 1444–1457
- [12] Grace H P 1982 *Chem. Eng. Commun.* **14** 225–277
- [13] Elemans P H M, Bos H L, Janssen J M H and Meijer H E H 1993 *Chem. Eng. Sci.* **48** 267–276
- [14] Delaby I, Ernst B and Muller R 1995 *Rheol. Acta* **34** 525–533
- [15] Patlazhan S A, Kravchenko I V, Muller R, Hoarau Y, Remond Y and Berlin A A 2016 *Dokl. Phys. Chem.*
- [16] Weller H G, Tabor G, Jasak H and Fureby C 1998 *Comput. Phys.* **12** 620–631
- [17] Boughamoura A, Abbassi H and Ben Nasrallah S 2003 *Comput. Mech.* **30** 410–420
- [18] Loux C, Bouchet G, Bouquey M and Muller R 2014 *Polym. Ing. Sci.* **54** 2046–2056